Crystallization of colloidal hard spheres under gravity

Matthieu Marechal and Marjolein Dijkstra
Soft Condensed Matter, Debye Institute for NanoMaterials Science, Utrecht University, Princetonplein 5, 3584 CC Utrecht, The Netherlands
(Received 3 April 2007; published 22 June 2007)

Using grand canonical Monte Carlo simulations, we study the crystallization of colloidal hard spheres under gravity. More specifically, we investigate the nature of the freezing transition as a function of gravity and chemical potential of the hard spheres. We find a discontinuous freezing transition where several fluid layers close to the bottom of the sample freeze simultaneously, i.e., at the same chemical potential. We also find that the number of layers that freezes at the same chemical potential decreases for higher gravitational field strength. Upon increasing the chemical potential further, the crystalline film thickness increases continuously.

DOI: 10.1103/PhysRevE.75.061404 PACS number(s): 82.70.Dd, 64.70.Dv, 61.20.Ja

I. INTRODUCTION

The bulk phase behavior of hard spheres has been studied in great detail and is well understood by now. In particular, it was shown by computer simulations that such a system shows a purely entropy-driven phase transition from a disordered fluid phase to a face-centered-cubic (fcc) crystal phase at sufficiently high densities [1]. Although the fcc phase is the most stable phase, the free energy difference with respect to the metastable hexagonal-close-packed (hcp) structure is only very small and is on the order of $10^{-4}k_BT$ per particle at the melting transition [2]. Here we define k_B as Boltzmann's constant and T the temperature. The crystallization of hard spheres at flat walls has also been the subject of many studies. It has been shown that a smooth hard wall causes pronounced layering of the fluid phase at the wall, which can lead eventually to prefreezing and complete wetting by the hard-sphere crystal upon increasing the density towards bulk coexistence [3–5]. Confining the hard-sphere system between two parallel hard walls leads to an intriguing sequence of capillary freezing and capillary melting transitions upon increasing the distance between the two walls and the formation of many different crystal structures such as square, triangular, rhombic, buckling, and prism phases [6,7]. Prefreezing or epitaxial crystal growth was also observed for walls with a surface pattern that is similar in symmetry to one of the crystal planes [8]. Using templates that are characteristic for the hcp crystal structure, i.e., templates that induce the ABAB stacking of the hexagonal layers perpendicular to the wall, the hcp crystal, which is metastable in bulk, has been grown experimentally in suspensions of colloidal particles [9,10]. These suspensions can serve as excellent experimental realizations of the hard-sphere system as the effective interactions of the colloids can be tuned in such a way that the particles interact approximately as hard spheres. However, gravity is often non-negligible in colloidal suspensions, as the gravitational energy becomes comparable to the thermal energy for colloid sizes of about a micrometer. Hence, a spatial inhomogeneous suspension is obtained due to the gravitational field, which is characterized by a density profile $\rho(z)$ that varies with altitude z. The parameter that is associated with a gravitational field is the so-called gravitational length and reads $\ell/\sigma=(\beta mg\sigma)^{-1}$, where m is the effective or buoyancy mass of the colloidal particles, $\beta=(k_BT)^{-1}$, σ the diameter of the colloids, and g the gravitational acceleration. Typically, ℓ/σ is of the order of $10^{-1}-10^{3}$ for colloidal particles. The density profile $\rho(z)$ follows from a competition between minimal energy (all colloids at the bottom) and maximum entropy (a homogeneous distribution in the available volume). In the case of a very dilute colloid concentration or at high altitude, where the suspension becomes sufficiently dilute, the system behaves similar to an ideal gas and the system obeys the Boltzmann distribution, yielding an exponential density profile with a decay length given by ℓ. In 1910, Perrin measured such a density profile under the microscope which enabled him to determine Boltzmann's constant and hence, Avogadro's number [11]. However, when the interactions become important, the density profile becomes highly nonexponential. Density profiles for hard spheres have been calculated using density functional theory and simulations [12–19], and are measured by light scattering techniques [20,21] and confocal microscopy in suspensions of colloidal hard spheres [22]. The measured concentration profiles obtained from a single experiment or simulation can be inverted to obtain the osmotic equation of state over a whole range of densities [12,20,21,23]. Crystallization in sedimentation profiles of hard spheres was studied using Monte Carlo simulations and density functional theory [13–17,19]. The simulations in Ref. [13] show a discontinuous transition where two layers crystallize at the same gravitational field strength. Upon increasing the gravitational field further, the crystalline film grows continuously. However, density functional theory predicts a discontinuous crystal growth via layering transitions upon increasing gravity, in contrast with the simulation results [13].

In this paper we investigate in more detail the nature of the freezing transition in suspensions of hard spheres as a function of chemical potential while keeping the gravitational field strength fixed. In Ref. [13], crystallization was studied as a function of gravity. However, in order to study the phase behavior of colloids in an external field, it is more convenient to treat the system grand canonically and to study the freezing transition as a function of chemical potential for a fixed value of the gravitational field strength [24]. Moreover, keeping the gravitational length of the particles fixed is closer to the experimental situation as the experimental ℓ is

determined by system parameters that are often constant in an experiment. To be more specific, ℓ depends on the gravitational acceleration, which is often equal to the value on earth, and on the buoyancy mass m, which is related by Archimedes' principle to $m=m_0-\tilde{\rho}v$ with $\tilde{\rho}$ the mass density of the solvent, m_0 the bare mass of the colloidal particles, and v the particle volume. Our results show a discontinuous freezing transition where a number of layers freezes at the same chemical potential. Upon increasing the chemical potential further, the crystalline film thickness increases continuously. It is important to stress that Monte Carlo simulations give only information about the equilibrium structure and not on the crystallization kinetics. The paper is organized as follows. In Sec. II we describe the model. In Sec. III, we present our Monte Carlo simulation results and we end with some concluding remarks in Sec. IV.

II. MODEL

We consider a system of hard spheres with diameter σ in a gravitational field oriented along the z direction. In addition, the spheres are confined between two smooth hard parallel walls at $z=0$ and $z=H$. The spheres are subjected to the external potential:

$$\phi(z)=\begin{cases} mgz, & \sigma/2 \leqslant z \leqslant H-\sigma/2, \\ \infty, & \text{otherwise}, \end{cases} \tag{1}$$

where z is the vertical coordinate, g is the gravitational acceleration, and m the buoyant mass of the hard spheres. The height H is chosen such that the density at $z=H-\sigma/2$ is sufficiently small, i.e., $\rho\sigma^3<10^{-6}$, and thus the system can be considered to be infinite in the z direction. The lateral dimensions of the box are $L_x=9a_0n$ and $L_y=10a_0n\sqrt{3}/2$ with n an integer. Note that the lateral dimensions of the simulation box are nearly equal, which minimizes the finite-size effects for the fluid phase and accommodates a hexagonal crystalline layer [the (111) plane of a fcc crystal] with lattice constant a_0. We employ periodic boundary conditions in the lateral dimensions and we use $n=2$ in our simulations.

III. RESULTS AND DISCUSSION

First, we perform Monte Carlo (MC) simulations in the canonical ensemble, i.e., we fix the number of particles $N=2004$, the area $A\equiv L_x\times L_y=18a_0\times 10\sqrt{3}a_0$ in the x and y direction, and the height H of the box. Moreover, we fix the strength of the gravitational field or the inverse gravitational length $g^*\equiv mg\sigma/k_BT=(\ell/\sigma)^{-1}$. The thermodynamic parameter that was defined in Ref. [13] is the mean area $\rho_A^*\equiv N\sigma^2/A$, which equals the number of particles per unit area of the bottom of the sample. The pressure at the bottom of the sample, i.e., at $z=0$, is directly related to ρ_A^*, as the pressure is determined by the gravitational force of all the spheres per unit area, i.e., $\beta P(z=0)\sigma^3=g^*\rho_A^*$. In our simulations, we measure the dimensionless density profile

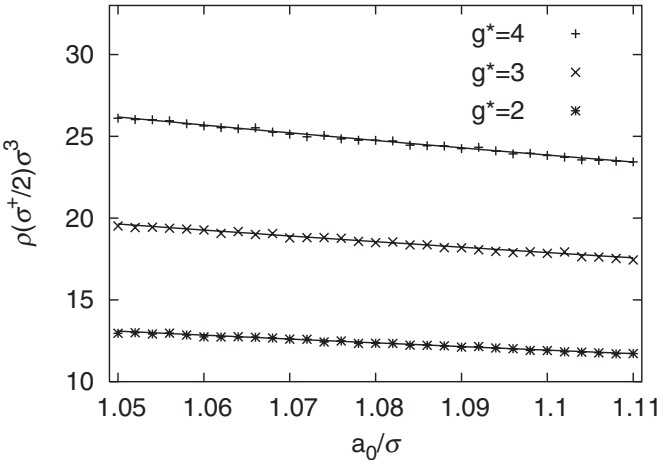

FIG. 1. The contact density $\rho(\sigma^+/2)\sigma^3$ as a function of the lattice constant a_0 of the crystal at the bottom of the sample for varying gravity $g^*=mg\sigma/k_BT=2$, 3, and 4. The error in the data is smaller than the size of the symbols. The solid lines denote the pressure at the bottom of the sample given by $\beta P(z=0)\sigma^3=g^*\rho_A^*$, where $\rho_A^*\equiv N\sigma^2/A$.

$$\rho(z)=\frac{1}{A}\int\int dxdy\rho(x,y,z)=\frac{1}{A}\left\langle\sum_{i=1}^{N}\delta(z-z_i)\right\rangle, \tag{2}$$

where $\rho(x,y,z)$ is the local density and the brackets denote an ensemble average. It is well known that for any one-component fluid near a hard wall, the contact density $\rho(\sigma^+/2)$ satisfies the sum rule $\rho(\sigma^+/2)=\beta P(z=0)$. The starting configurations that we use in our simulations consist of a face-centered-cubic (fcc) crystal structure with the (111) axis normal to the bottom of the sample and with varying lattice constant a_0. In Ref. [13], the contact theorem was employed to obtain the "correct" a_0. These authors found that the sum rule was only satisfied for a lattice constant $a_0=1.088\sigma$. In Fig. 1, we plot the contact density $\rho(\sigma^+/2)\sigma^3$ as a function of a_0 for $g^*=2$,3, and 4. For comparison, we also plot $\beta P(z=0)\sigma^3$ denoted by the solid lines. Figure 1 shows that the sum rule is satisfied for all values of the lattice constants we considered, i.e., $1.04\leqslant a_0/\sigma\leqslant 1.11$. Hence, we are not able to obtain the "correct" lattice constant by requiring consistency of the bottom pressure with the contact density.

In order to solve this problem, we perform Monte Carlo simulations in the grand-canonical ensemble, i.e., we fix the chemical potential $\mu^*\equiv\beta\mu-\ln(\Lambda^3/\sigma^3)$ and the volume of the box. Due to particle removals and insertions in a grand-canonical Monte Carlo simulation, the system equilibrates more easily to the equilibrium crystal structure by relaxing the stress and strain in the crystal and adapting the lattice constant. Hence one does not have to estimate the equilibrium value for the lattice constant beforehand as in the case of Monte Carlo simulations in the canonical ensemble. Moreover, it proves more convenient to study phase behavior in inhomogeneous systems in the grand-canonical ensemble in order to ensure equal chemical potential in coexisting phases [24].

We perform grand-canonical Monte Carlo simulations for varying values of gravity $g^*=1$, 2, 3, and 4. The box shape is

set by $a_0=1.11$ and $n=2$. We checked that simulation runs with larger box sizes and different box shapes show the same results within the statistical error. The crystal can adapt itself to the "correct" lattice constant by changing slightly the crystal orientation, as can be seen in Fig. 4. In each Monte Carlo cycle we perform with a probability $\mathcal{P}_{\text{exch}}$ an attempt to exchange a particle with an ideal reservoir and otherwise an attempt to displace a particle. We use $\mathcal{P}_{\text{exch}}=0.5$ or 0.9. The maximum displacement in each direction was 0.1 if $\mathcal{P}_{\text{exch}}=0.5$ and 0.2 if $\mathcal{P}_{\text{exch}}=0.1$. A simulation run consists of 1.6×10^{10} ($\mathcal{P}_{\text{exch}}=0.1$) or 8×10^{9} ($\mathcal{P}_{\text{exch}}=0.5$) MC cycles to thermalize the system and twice as many cycles for the production runs to sample the statistical averages of interest. The number of trial moves to displace a particle was always larger than 8×10^{5} per particle.

We study both crystallization and melting. In the first case, the initial condition is a dilute cubic crystal which melted within 10^6 MC cycles. We also start with an fcc crystal phase to study melting. We checked that our simulation results did not depend on the starting configuration. However, the equilibration of the system is about 10 times longer near the freezing transition.

In Fig. 2, we show density profiles for hard spheres in a gravitational field with strength $g^*=1$, 2, 3, and 4. The profiles were averaged in bins of width $\delta z=0.01\sigma$. For each g^*, we show density profiles at $\mu^*=14$, at a value of μ^* just above the freezing transition of the first layer, and at $\mu^*=25$. At $\mu^*=14$, we find density profiles of a liquid phase with pronounced layering of the fluid phase at the lower wall. Upon increasing μ^* just above the value at the freezing transition of the first fluid layer, we observe the formation of crystalline layers at the bottom: $\rho(z)$ drops to zero between the density peaks close to the wall. At $\mu^*=25$, we find for all g^* the formation of several crystalline layers at the wall. From Fig. 2 we observe that the number of crystalline layers decreases upon increasing g^* at fixed μ^*. This trend is to be expected since an infinite number of crystalline layers are expected to be formed for zero gravity and a chemical potential μ^* fixed at its bulk value, i.e., $\mu^*_{\text{coex}}=16.071$.

We now take a closer look at the crystallization of the fluid layers at the bottom wall. To this end, we measure the hexagonal bond order parameter profile,

$$\psi_6(z)=\frac{\left|\left\langle\sum_{i=1}^{N}\psi_{6,i}\delta(z-z_i)\right\rangle\right|}{\left\langle\sum_{i=1}^{N}\delta(z-z_i)\right\rangle}. \tag{3}$$

Here the hexagonal bond order parameter of particle i is defined as

$$\psi_{6,i}=\frac{1}{N_i}\sum_{j=1}^{N_i}\exp 6\imath\theta_{ij}, \tag{4}$$

where the sum over j is over the N_i nearest neighbors of particle i, θ_{ij} is the angle between $\mathbf{r}_{ij}\equiv\mathbf{r}_i-\mathbf{r}_j$ and some arbitrary axis in the horizontal plane, and $\imath$ (without dot) is the

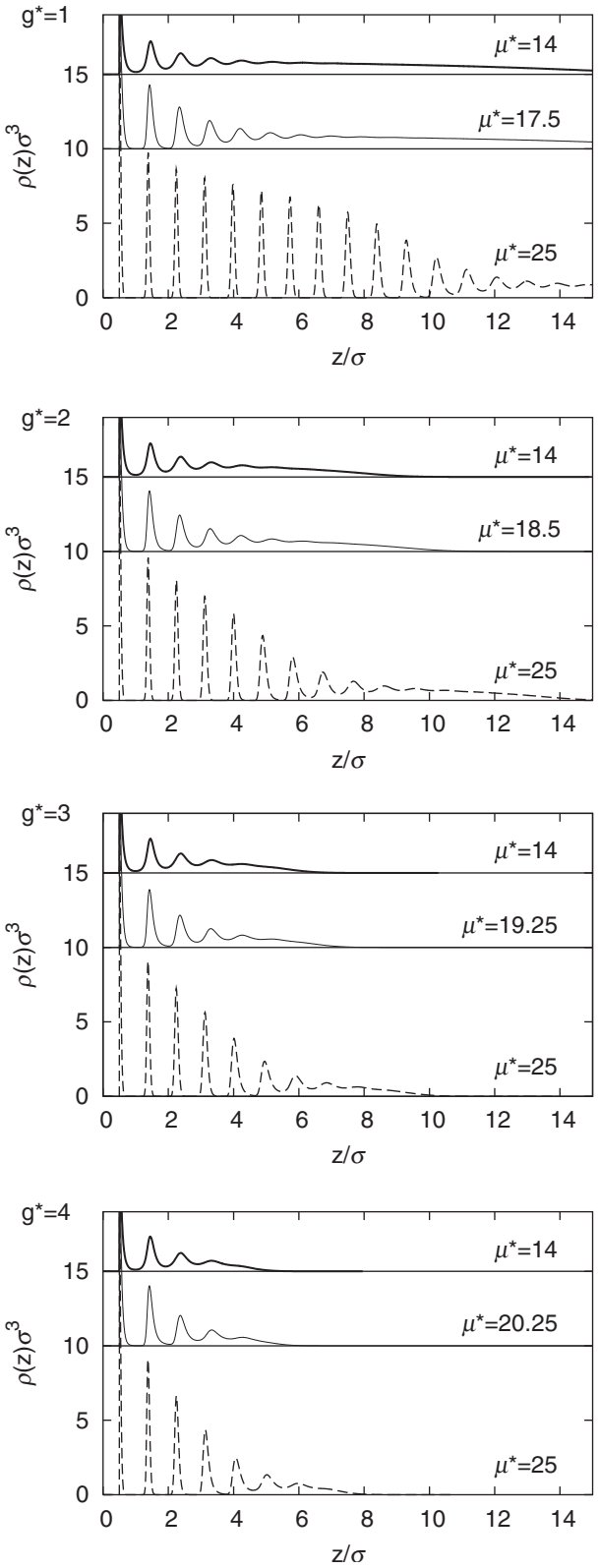

FIG. 2. Density profiles $\rho(z)$ for hard spheres in a gravitational field with strength $g^*=1$ (top), 2, 3, and 4 (bottom). For each g^*, density profiles are shown for a fluid phase ($\mu^*=14$, thick solid line), just above the freezing transition of the first layer ($14\leqslant\mu^*\leqslant25$, thin solid line), and a fluid with crystalline layers at the bottom ($\mu^*=25$, dashed line). The results are shifted vertically for clarity of display.

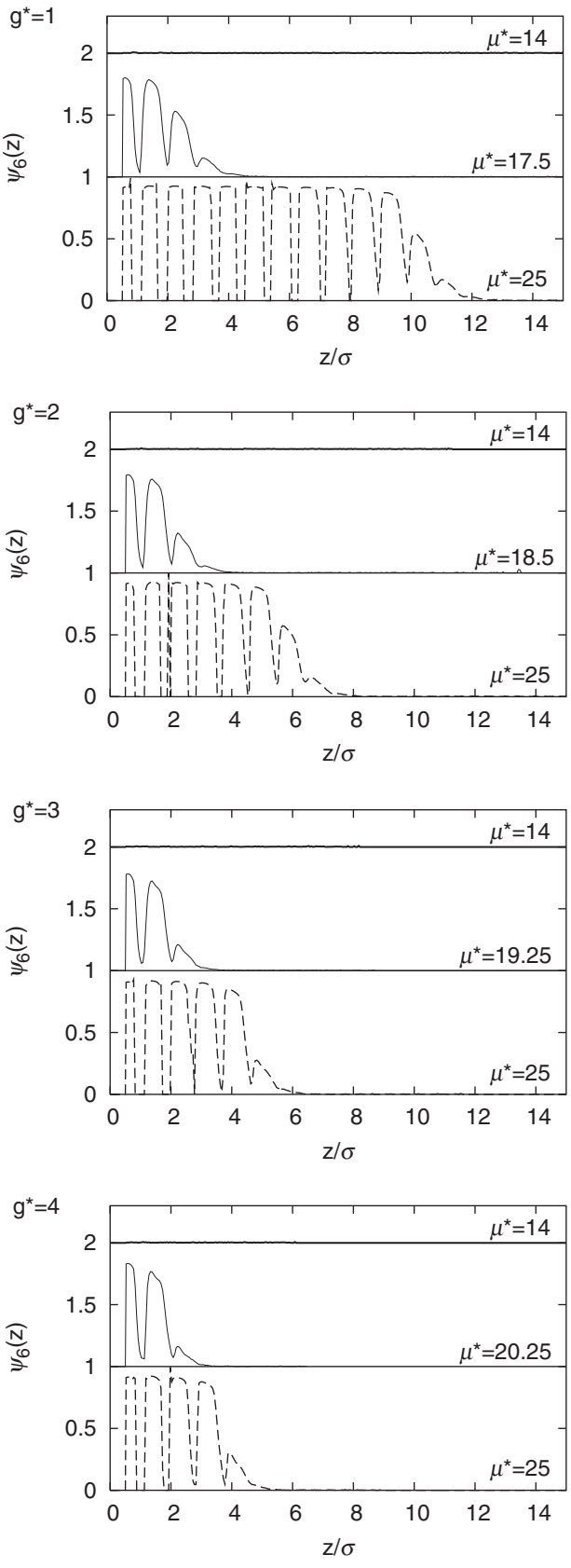

FIG. 3. Hexagonal bond order parameter profiles $\psi_6(z)$ for hard spheres in a gravitational field. Profiles are shown for the same state points as in Fig. 2. The results are shifted vertically for clarity of display. For $\mu^*=14$, we find $\psi_6(z)=0$.

imaginary number. Particles i and j were considered nearest neighbors when they satisfied $x_{ij}^2+y_{ij}^2+4z_{ij}^2<(1.3a_0)^2$. Due to the factor 4, this condition preferably selects nearest neighbors, which lie within one layer.

Examples are plotted in Fig. 3 for the same state points as in Fig. 2. For $\mu^*=14$, we find a flat hexagonal bond order parameter profile, i.e., $\psi_6(z)=0$ for all values of z. For a value of μ^* slightly above the freezing transition of the first layer, we observe clearly that the first and second layers crystallize at the same chemical potential for all values of g^* considered here. We also find a discontinuous jump in the hexagonal bond order of the third layer at this chemical po-

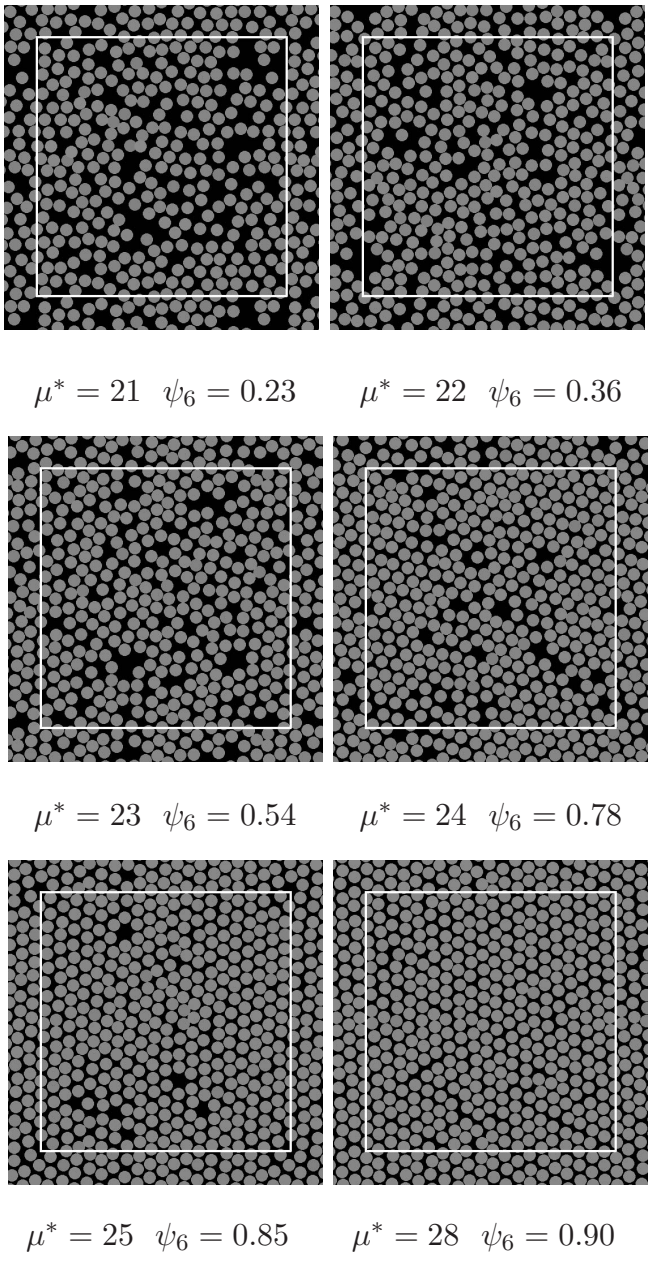

FIG. 4. Typical configurations of the third fluid layer in a system of hard spheres in a gravitational field with strength $g^*=4$. The white rectangle denotes the horizontal box area. Some periodic images of the particles are shown as well.

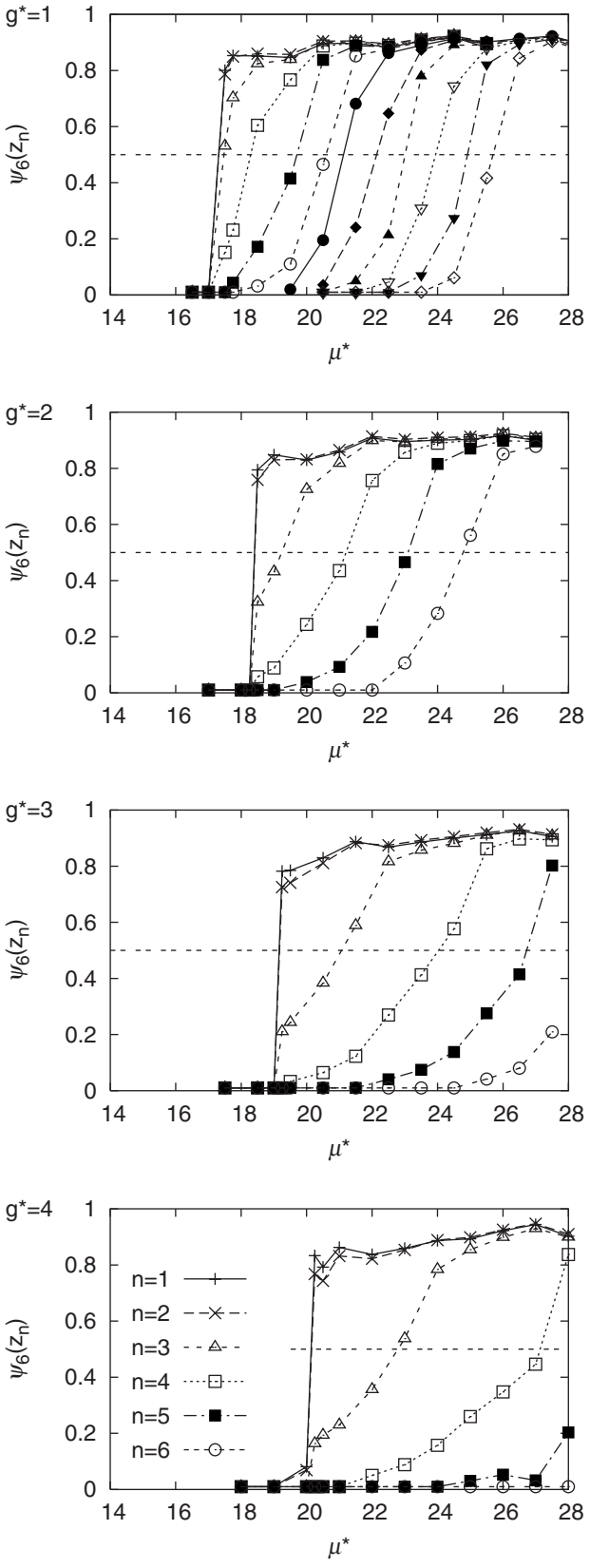

FIG. 5. The maximum hexagonal bond order parameter in the nth layer as a function of chemical potential μ^* for a system of hard spheres in a gravitational field with strength $g^*=1$, 2, 3, and 4. The horizontal dashed line denotes our crystallinity criterion $\psi_6(z_n)>0.5$.

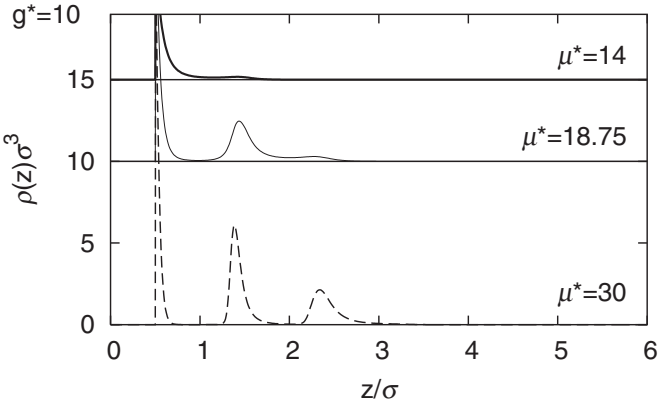

FIG. 6. Density profiles $\rho(z)$ for hard spheres in a gravitational field with strength $g^*=10$ at varying values of the chemical potential. The results are shifted vertically for clarity of display.

tential, although the jump is much smaller than that of the first two layers. The jump in ψ_6 of the third layer increases upon decreasing g^*. Upon increasing μ^* further, the hexagonal bond order ψ_6 of the nth layer with $n \geqslant 3$ increases continuously within each layer. First, the layer is fluidlike, i.e., ψ_6 is low. As μ^* increases, we observe the presence of crystallites, which merge and form a crystal with many defects upon further increase of μ^*. At very high chemical potential, the defects will be annealed out, resulting in a high value of ψ_6. In Fig. 4, we show typical configurations of the third layer of a fluid of hard spheres in a gravitational field with strength $g^*=4$ and increasing values of μ^*.

The nth maximum of ψ_6 is a measure for the crystalline order in the nth layer. These maxima are plotted for the first six layers in Fig. 5. Again our results suggest a discontinuous freezing transition of the first two layers at the same chemical potential, and, upon increasing μ^*, additional layers crystallize continuously. We also observe a discontinuous jump in ψ_6 of the third layer at the same μ^*. If we adopt the criterion that a layer is crystalline if $\psi_6(z_n)>0.5$ with z_n the nth local maximum of $\psi_6(z)$, we can conclude that the number of layers that freeze at the same chemical potential equals 3 for $g^*=1$ and 2 for $g^*=2$, 3, and 4. Our results show that the number of layers that crystallizes simultaneously, i.e., at the same μ^*, increases for decreasing g^*. As already mentioned before, this finding can be explained by the fact that an infinite number of crystalline layers will be formed at zero gravity and at a chemical potential equal to its bulk value μ^*_{coex}. It is tempting to argue that for low g^* three or more layers will crystallize at the same μ^*. A natural question to ask is whether the first and second layers always crystallize at the same μ^*. To this end, we perform simulations at $g^*=10$. The resulting density profiles are plotted in Fig. 6. In Fig. 7, we plot the maximum hexagonal bond order parameter for the first four layers as a function of μ^*. Our results indicate a first-order freezing transition of the first layer, and a continuous freezing transition of the second and third layers at higher μ^*. To summarize, we expect that the number of layers that crystallizes simultaneously at the same chemical potential with a first-order phase transition increases from 1 to ∞ upon lowering the gravitational field strength.

In Fig. 8, we plot the freezing transitions for the first six layers as a function of g^* and μ^* using our crystallinity cri-

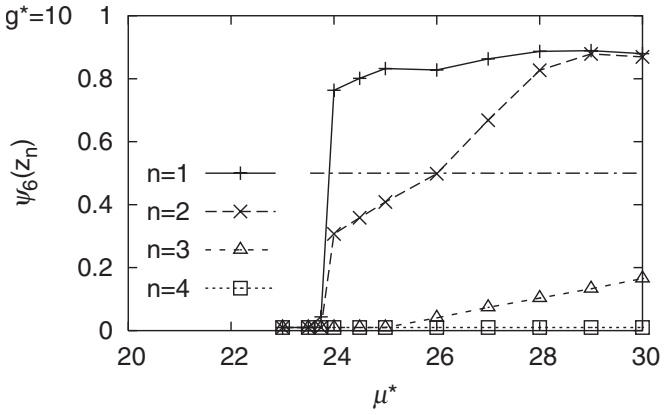

FIG. 7. The maximum hexagonal bond order parameter in the nth layer as a function of chemical potential μ^* for hard spheres in a gravitational field with strength $g^*=10$. The horizontal dashed line denotes our crystallinity criterion $\psi_6(z_n)>0.5$.

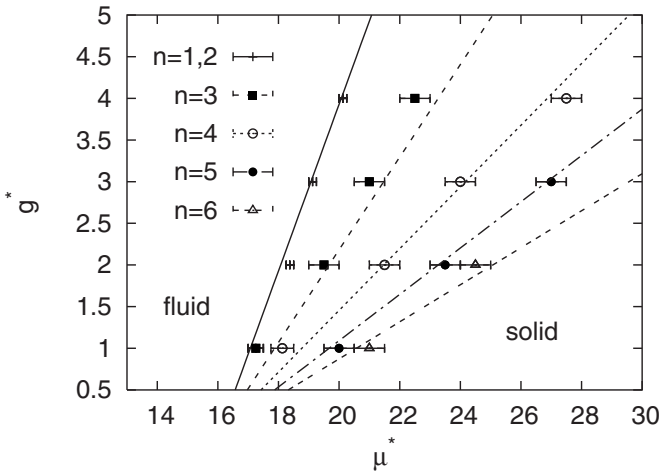

FIG. 8. Phase diagram of the freezing transitions of the first six layers as a function of μ^* and g^* as obtained from simulations (symbols). The lines denote our prediction for the freezing transitions $\mu^*_{\rm int}(z_n')\simeq\mu^*_{\rm coex}=16.071$ with z_n' given by Eq. (6). The solid line denotes a first-order freezing transition, while the dashed lines denote continuous transitions.

terion $\psi_6(z_n')>0.5$. The total chemical potential at height z for a system of hard spheres in a gravitational field reads $\mu^*=\mu^*_{\rm int}(z)+g^*z/\sigma$, where $\mu^*_{\rm int}(z)$ is the internal chemical potential, i.e., the chemical potential the system would have, if there is no external potential. One expects that the fluid at height z crystallizes if $\mu^*_{\rm int}(z)\simeq\mu^*_{\rm coex}$. In Fig. 8 we compare our results for freezing of the first six layers with the estimate that the nth layer crystallizes when

$$\mu^*_{\rm int}(z_n')=\mu^*-g^*z_n'/\sigma\simeq\mu^*_{\rm coex}, \tag{5}$$

where we use that z_n' is the z position of the $(n-1)$th local minimum of $\rho(z)$, which corresponds to the minimum just below the nth layer. For the freezing transition of the first and second layers we use, however, that z_n' is given by the first local minimum, which lies in between the first and second layers,

$$z_n'/\sigma=\begin{cases}1.0, & n=1,2,\\ 0.9\times(n-1), & n>2.\end{cases} \tag{6}$$

Note that the predictions are denoted by dashed lines for $n>2$, corresponding to a continuous freezing transition, while for $n=1,2$ the first-order freezing transition is denoted by a solid line. As the simulation results for the freezing transition of the different fluid layers agree well with these predictions, we can conclude that the nth layer for $n\geqslant 2$ is crystalline not because the chemical potential at this height is higher than $\mu^*_{\rm coex}$, but because the chemical potential of the $(n-1)$th layer is sufficiently high that this layer is fully crystalline. This layer then acts as a template for the nth layer, resulting in crystallization of this layer [28].

For $g^*=10$, Eq. (5) with $z_1'/\sigma=1$ as obtained from Eq. (6) for $n=1$ predicts that the first layer freezes at a chemical potential $\mu^*=26.07$. Figure 7 shows, however, that the crystallization of the first layer occurs at $\mu^*\simeq 24$, which corresponds to a height $z_1'/\sigma=0.8$. This is closer to the position of the first layer itself, rather than the minimum between the first and the second layers. Reassuringly, the crystallization of the second layer does occur at $\mu^*\simeq 26$. Apparently, our prediction (6) only holds for a phase transition from a fluid phase to a stable ordered phase consisting of two crystalline layers, while it fails for $g^*=10$, where we observe a transition from a fluid phase to a phase with only one frozen layer. Hence, one would also expect that if the freezing transition involves a phase with three or more crystalline layers (at $g^*\leqslant 1$), the freezing transition occurs at a different μ^* than predicted by Eq. (6). The value of μ^* at the discontinuous freezing transition will probably correspond to a (weighted) average of all the layers that crystallize. However, the error bars in Fig. 8 are too large to confirm this conjecture.

In order to compare our results to earlier work we calculate the pressure at the bottom $P_0^*=\beta P(z=0)\sigma^3$ of the sample and the pressure on the first layer $P_1^*=\beta P(z=z_1')\sigma^3$,

$$P_0^*=\frac{\langle N\rangle\sigma^2g^*}{A} \tag{7}$$

and

$$P_1^*=\frac{(\langle N-N_1\rangle)\sigma^2g^*}{A}, \tag{8}$$

where N_1 is the number of particles in the first layer. Table I displays P_0^* and P_1^* at the freezing transition of the first (and second) layer of our simulations. In Ref. [26], it was argued

TABLE I. The pressure at the bottom $P_0^*=\beta P(z=0)\sigma^3$ and the pressure on the first layer $P_1^*=\beta P(z=z_1')\sigma^3$ at the freezing transition of the first layer for gravity $g^*=1$, 2, 3, and 4. For comparison, we also show results from experiments [22] and simulations [13].

	Expt. [22]	Sim. [13]	Our work			
g^*	1.2	2.625	1.0	2.0	3.0	4.0
P_0^*	14.0	14.25	12.6	13.4	14.3	15.3
P_1	—	—	11.8(3)	11.6(2)	11.6(3)	11.5(1)

that the first bottom layer will crystallize when $\beta P(z=\sigma/2)\sigma^3$ reaches the bulk pressure at coexistence $\beta P_{\mathrm{coex}}\sigma^3=11.56$ [27]. However, we observe that P_0^* depends on g^* and is always $>\beta P_{\mathrm{coex}}\sigma^3$, while P_1^* is independent of g^* and equals $\beta P_{\mathrm{coex}}\sigma^3$ within the error bars. A similar result was obtained using density functional theory and kinetic theory [14,15], where a linear behavior between $\langle N\rangle\sigma^2/A$ and g^* was found for the freezing transition. For comparison, we also show P_0^* for previous simulations [13] and experiments [22], which are in reasonable agreement with our simulations.

Finally, we investigate the lattice constant of the bottom layer as a function of μ^* and g^*. In our simulations, we determine the lattice constant of the nth layer by

$$a_n=\sqrt{\frac{2A}{\sqrt{3}\langle N_n\rangle}}, \tag{9}$$

where we assumed a triangular symmetry for the crystal layer and where $\langle N_n\rangle$ is the number of particles in layer n, which is calculated by

$$\langle N_n\rangle=A\int_{z_n}^{z_{n-1}}\rho(z)dz. \tag{10}$$

We plot in Fig. 9 the lattice constant of the first layer a_1 as a function of the chemical potential μ^* for gravitational field strengths $g^*=1$, 2, 3, and 4. For comparison, we also plot the lattice constant of a bulk crystal at μ^* using Speedy's equation of state [25]. We clearly observe in Fig. 9 that the simulation results for a_1 are much higher than those of the corresponding bulk crystal. Upon closer inspection, we find that the lattice constants a_n for $n>1$ are all equal to a_1 within the statistical error for all values of μ^* and g^* we considered. This finding is remarkable as the pressure varies enormously with height. As the lattice constants in all the layers are the same, all layers must adjust to each other. Consequently, one might expect that the lattice constant is determined by an average over all layers which have a chemical potential $\mu_{\mathrm{coex}}^*\leqslant\mu\leqslant\mu^*$,

$$\bar{a}_{\mathrm{bulk}}(\mu^*)=\frac{\int_{\mu_{\mathrm{coex}}^*}^{\mu^*}a_{\mathrm{bulk}}(\mu)d\mu}{\mu^*-\mu_{\mathrm{coex}}^*}. \tag{11}$$

Figure 9 shows that the agreement between the simulations and this expression has been improved. However, this expression still underestimates the observed lattice constant systematically. This effect is caused by "crystalline" layers with a high ψ_6, for which $\mu_{\mathrm{int}}(z)<\mu_{\mathrm{coex}}^*$. Ignoring these layers with a relatively low $\mu_{\mathrm{int}}(z)$ and hence a large lattice constant of the corresponding bulk crystal underestimates $\bar{a}_{\mathrm{bulk}}$ given by Eq. (11).

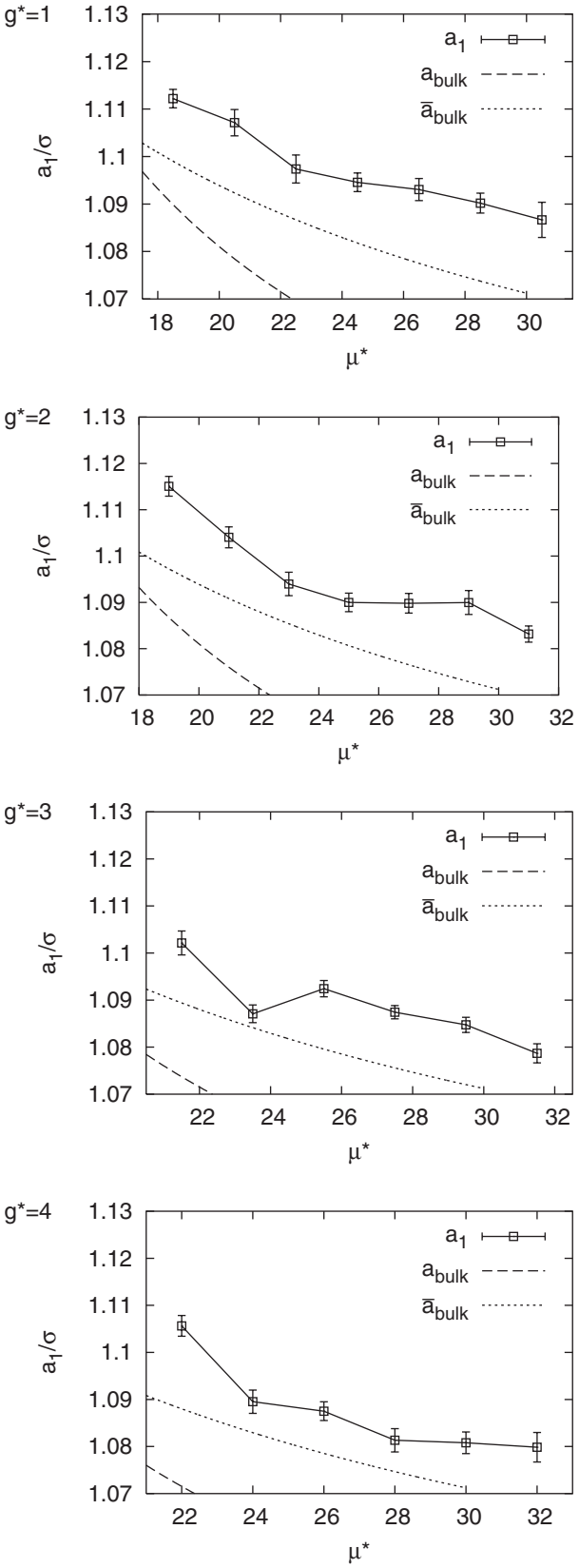

FIG. 9. Lattice constant of the first layer a_1 as function of the chemical potential for varying gravities: $g^*=1,2,3,4$ as obtained from simulations (□). The dashed lines denote the lattice constant of a bulk crystal at μ^*, while the short-dashed lines show an averaged lattice constant given by Eq. (11).

IV. CONCLUSIONS

We have investigated the nature of the freezing transition in sedimenting colloidal hard spheres. Our results provide evidence for a first-order freezing transition where several

fluid layers close to the bottom of the sample freeze at the same chemical potential. If the chemical potential is increased further, additional fluid layers will solidify continuously. We have determined a phase diagram of the freezing transitions of the first six fluid layers as a function of chemical potential and gravity using computer simulations, and we show that our simulation results agree well with a simple prediction given by Eq. (5) with Eq. (6). A better understanding of the mechanisms of crystallization is important both for a better insight in colloidal crystallization, as well as for advanced applications. For instance, sedimentation is often used as a method to grow large colloidal crystals for (photonic) applications [29–34]. We also note that the solidification of hard spheres under gravity has implications for granular matter systems [14,15,26].

ACKNOWLEDGMENT

This work was financially supported by the High Potential Programme of Utrecht University.

[1] W. W. Wood and J. D. Jacobson, J. Chem. Phys. **27**, 1207 (1957); B. J. Alder and T. E. Wainwright, *ibid.* **27**, 1208 (1957); W. G. Hoover and F. H. Ree, *ibid.* **49**, 3609 (1968).
[2] P. G. Bolhuis, D. Frenkel, S. C. Mau, and D. A. Huse, Nature (London) **388**, 235 (1997).
[3] D. J. Courtemanche and F. van Swol, Phys. Rev. Lett. **69**, 2078 (1992).
[4] D. J. Courtemanche, T. A. Pasmore, and F. van Swol, Mol. Phys. **80**, 861 (1993).
[5] M. Dijkstra, Phys. Rev. Lett. **93**, 108303 (2004).
[6] M. Schmidt and H. Löwen, Phys. Rev. Lett. **76**, 4552 (1996); Phys. Rev. E **55**, 7228 (1997).
[7] A. Fortini and M. Dijkstra, J. Phys.: Condens. Matter **18**, L371 (2006).
[8] M. Heni and H. Löwen, J. Phys.: Condens. Matter **13**, 4675 (2001).
[9] J. P. Hoogenboom, A. K. van Langen-Suurling, J. Romijn, and A. van Blaaderen, Phys. Rev. Lett. **90**, 138301 (2003).
[10] J. P. Hoogenboom, A. K. van Langen-Suurling, J. Romijn, and A. van Blaaderen, Phys. Rev. E **69**, 051602 (2004).
[11] J. Perrin, J. Phys. **9**, 5 (1910).
[12] T. Biben, J. Hansen, and J. Barrat, J. Chem. Phys. **98**, 7330 (1993).
[13] T. Biben, R. Ohnesorge, and H. Löwen, Europhys. Lett. **28**, 665 (1994).
[14] D. C. Hong, Physica A **271**, 192 (1999).
[15] J. A. Both and D. C. Hong, Phys. Rev. E **64**, 061105 (2001).
[16] W. Nuesser and H. Versmold, Mol. Phys. **96**, 893 (1999).
[17] A. Mori *et al.*, J. Chem. Phys. **124**, 174507 (2006).
[18] H. Chen and H. Ma, J. Chem. Phys. **125**, 024510 (2006).
[19] S.-C. Kim and S.-H. Suh, J. Phys.: Condens. Matter **15**, 6617 (2003).
[20] R. Piazza, T. Bellini, and V. Degiorgio, Phys. Rev. Lett. **71**, 4267 (1993).
[21] M. A. Rutgers, J. H. Dunsmuir, J. Z. Xue, W. B. Russel, and P. M. Chaikin, Phys. Rev. B **53**, 5043 (1996).
[22] J. P. Hoogenboom, P. Vergeer, and A. van Blaaderen, J. Chem. Phys. **119**, 3371 (2003).
[23] S. Hachisu and K. Tokano, Adv. Colloid Interface Sci. **16**, 233 (1982).
[24] R. Evans, Adv. Phys. **28**, 143 (1979).
[25] R. J. Speedy, J. Phys.: Condens. Matter **10**, 4387 (1998).
[26] Y. Levin, Physica A **287**, 100 (2000).
[27] D. Frenkel and B. Smit, *Understanding Molecular Simulation* (Academic Press, San Diego, 2002).
[28] M. Heni and H. Löwen, Phys. Rev. Lett. **85**, 3668 (2000).
[29] A. van Blaaderen, R. Ruel, and P. Wiltzius, Nature (London) **385**, 321 (1997).
[30] J. E. G. J. Wijnhoven and W. L. Vos, Science **281**, 802 (1998).
[31] P. V. Braun *et al.*, Adv. Mater. (Weinheim, Ger.) **13**, 721 (2001).
[32] A. A. Zakhidov *et al.*, Science **282**, 897 (1998).
[33] M. Holgado *et al.*, Langmuir **15**, 4701 (1999).
[34] A. Blanco *et al.*, Nature (London) **405**, 437 (2000).